Supplementary Information

High-Performance Flexible Thermoelectric Power Generator using Laser Multi-Scanning Lift-Off Process

Sun Jin Kim[†, ‖], *Han Eol Lee*[‡, ‖], *Hyeongdo Choi*[†], *Yongjun Kim*[†], *Ju Hyung We*[†], *Ji Seon Shin*[§], *Keon Jae Lee*[*,‡] *and Byung Jin Cho*[*,†]

[†]Department of Electrical Engineering, KAIST, 291 Daehak-ro, Yuseong, Daejeon 34141, Republic of Korea

[‡]Department of Materials Science and Engineering, KAIST, 291 Daehak-ro, Yuseong, Daejeon 34141, Republic of Korea

[§]Tegway Co. Ltd., #711 National Nano Fab., 291 Daehak-ro, Yuseong, Daejeon 34141, Republic of Korea

[‖] These authors contributed equally to this work.

[*]E-mail: bjcho@kaist.edu. Tel: +82-42-350-3485. Fax: +82-42-350-8565.

[*]E-mail: keonlee@kaist.ac.kr. Tel: +82-42-350-3343. Fax: +82-42-350-3310.

● **A procedure of screen-printed TE formation (cross-sectional view)**

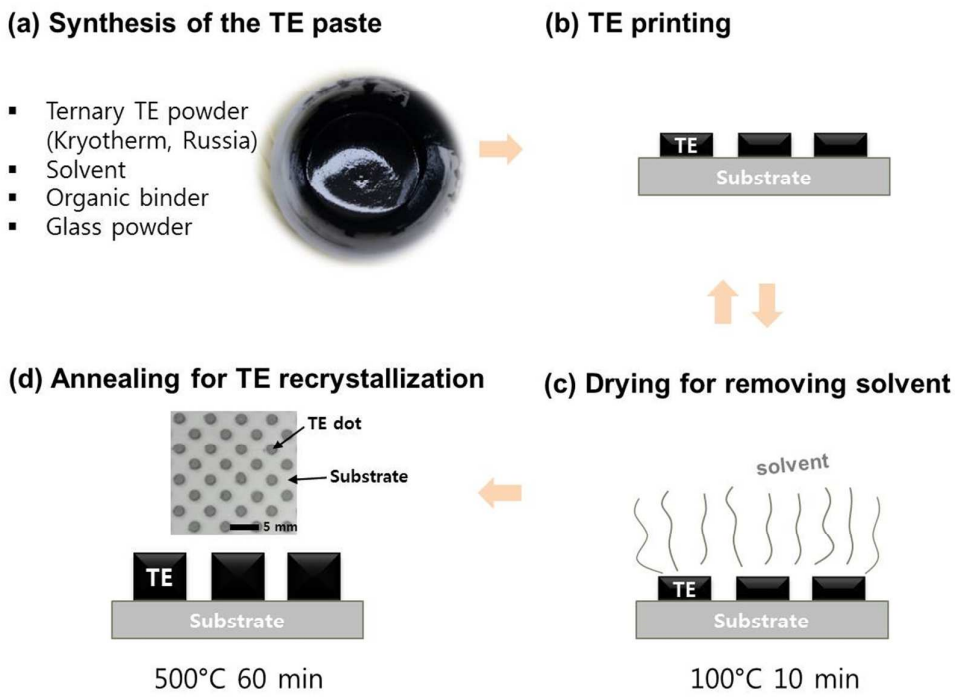

Figure S1. Schematic illustration of screen-printed TE formation. (a) Synthesis of the TE paste. (b) Printing process of the TE paste. (c) Drying process for removing solvent from the printed TE film. (d) Subsequent annealing process for TE recrystallization.

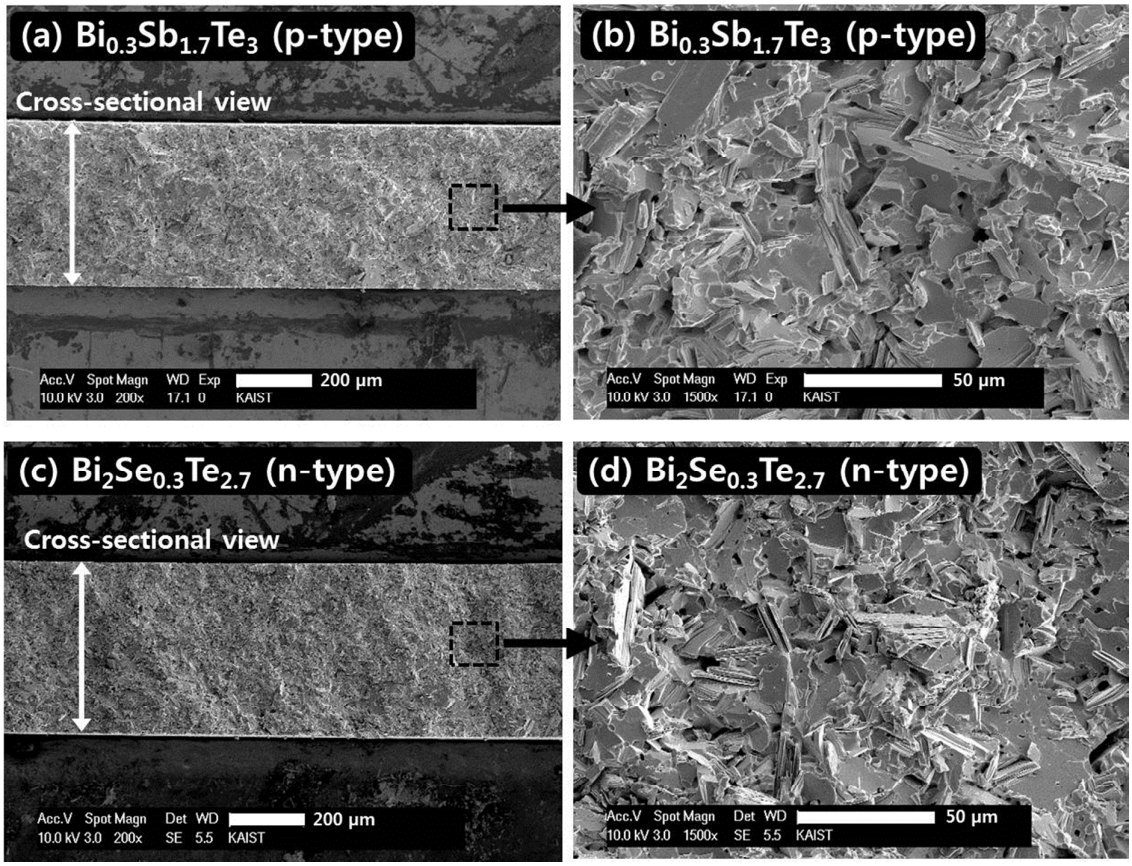

Figure S2. SEM images of the screen-printed TE thick films (cross-sectional views). (a)&(b) p-type $Bi_{0.3}Sb_{1.7}Te_3$ thick film (c)&(d) n-type $Bi_2Se_{0.3}Te_{2.7}$ thick film

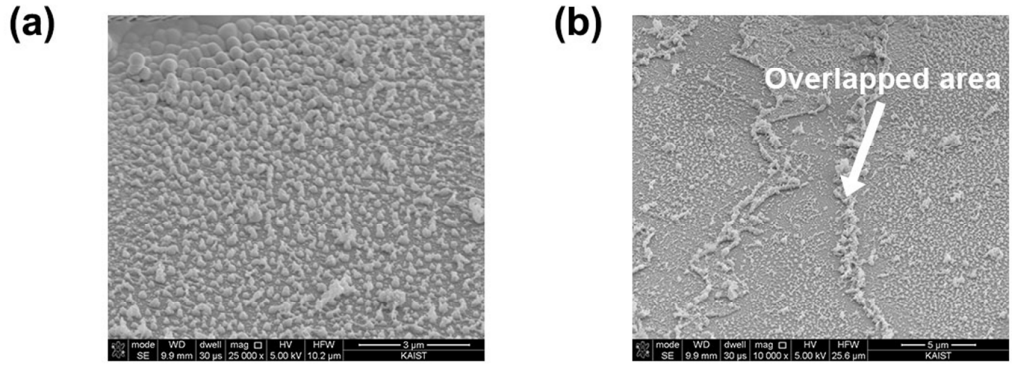

Figure S3. SEM images showing the surface of laser irradiated a-Si of (a) no overlapped and (b) overlapped area.

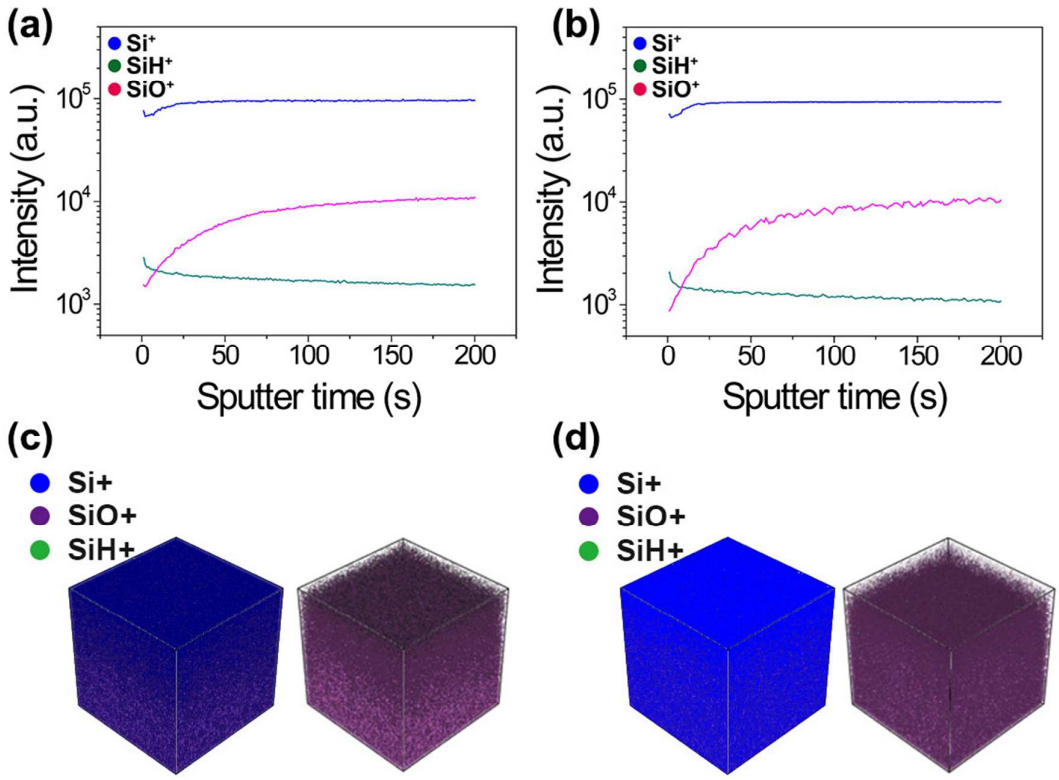

Figure S4. Surface analysis results of a-Si surface characterized by TOF-SIMS (a) before and (b) after LMS process. The graph shows the composition variation of the a-Si surface as a function of the sputtering time. 3-dimensional mapping image of a-Si surface (c) before and (d) after LMS process (blue: Si+, purple: SiO+, green: SiH+).

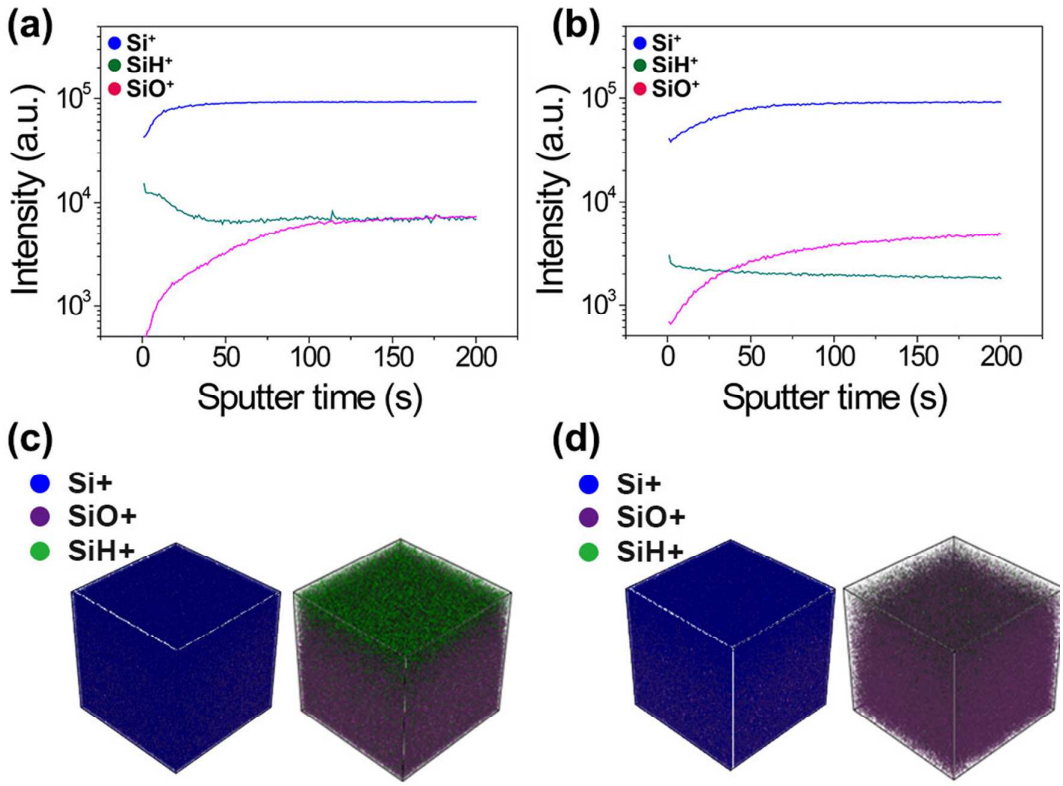

Figure S5. Surface analysis results of a-Si:H surface measured by TOF-SIMS (a) before and (b) after ILLO process. The graph shows the composition variation of the a-Si:H surface as a function of the sputtering time. 3-dimensional mapping image of a-Si:H (c) before and (d) after ILLO process (blue: Si+, purple: SiO+, green: SiH+).

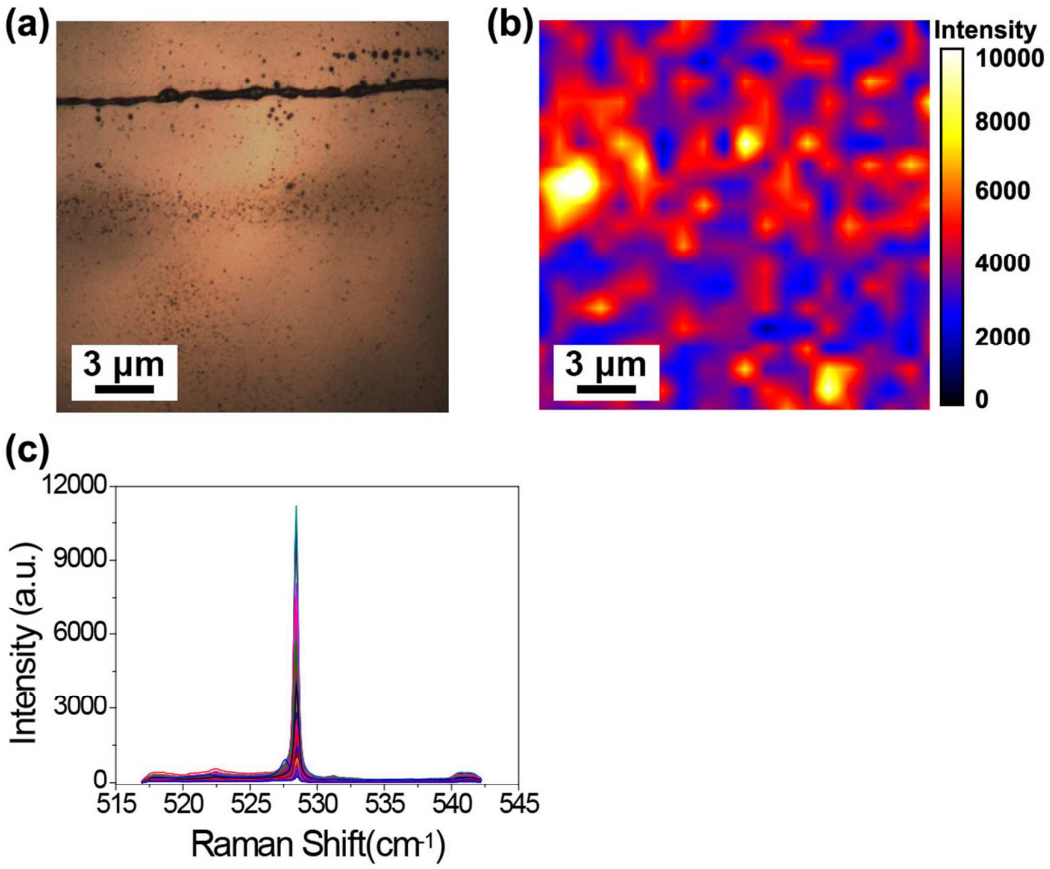

Figure S6. (a) Magnified optical image of the a-Si surface after LMS process. (b) Raman mapping image of same area with Fig.S4(a). (c) Raman spectra of the mapping data observed from a-Si thin film after LMS process. The peaks were measured in a surface area of 20×20 μm and indicated typical results of poly-Si.

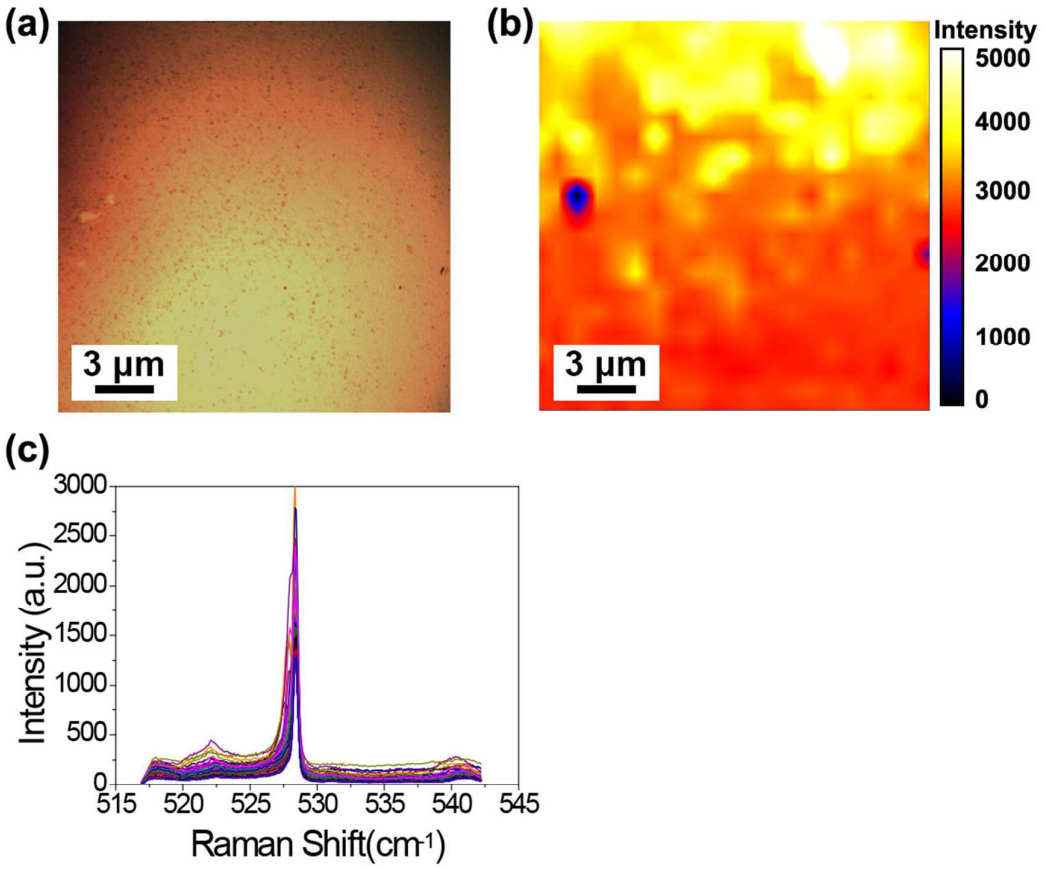

Figure S7. (a) Magnified optical image of the a-Si surface before LMS process. (b) Raman mapping image of same area with Fig.S5(a). (c) Raman spectra of the mapping data observed from a-Si thin film before LMS process. The peaks were measured in a surface area of 20×20 μm and indicated partially crystalized Si.

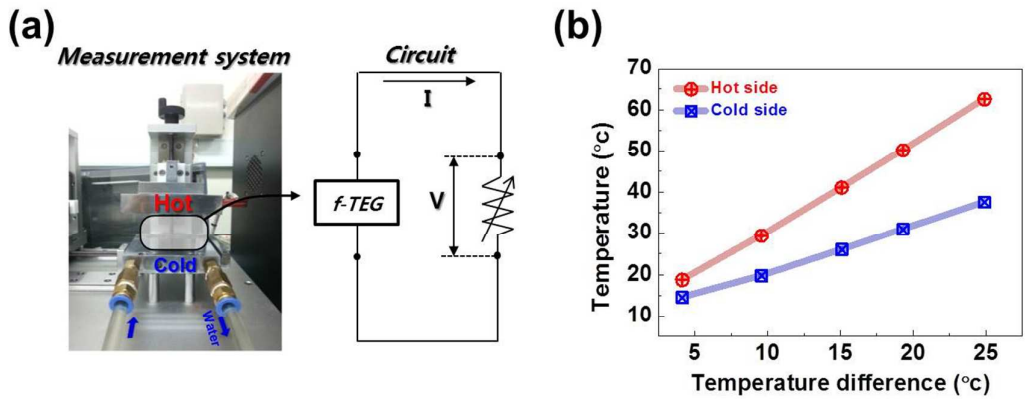

Figure S8. (a) Photograph and schematic illustration of the heating and cooling system with an electric circuit for evaluating output characteristics. (b) The temperature measured at hot and cold sides of the f-TEG.

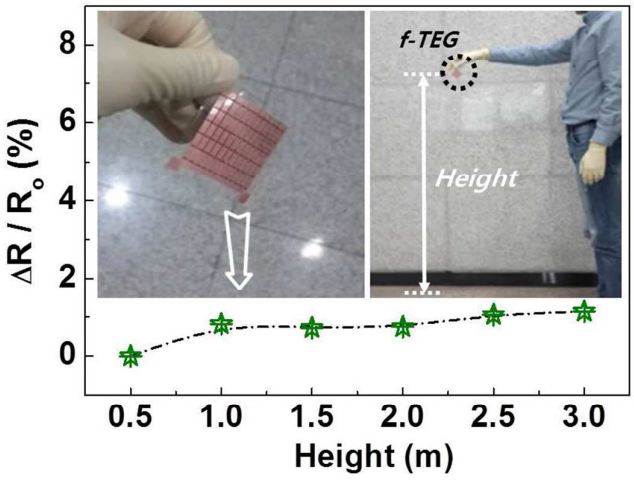

Figure S9. Drop test for verifying the mechanical stability after drop impact.

	Seebeck coefficient (μV/K)	Electrical conductivity (x10^4 S/m)	Thermal conductivity (W/m·K)	ZT
$Bi_{0.3}Sb_{1.7}Te_3$ [p-type]	184	6.86	0.84	0.80
$Bi_2Se_{0.3}Te_{2.7}$ [n-type]	134	7.86	0.86	0.49

Table S1. Thermoelectric properties of the screen-printed $Bi_{0.3}Sb_{1.7}Te_3$ and $Bi_2Se_{0.3}Te_{2.7}$ films.